Received: 26 September 2022 | Accepted: 24 May 2023

DOI: 10.1111/1365-2478.13383

Geophysical Prospecting | EAGE EUROPEAN ASSOCIATION OF GEOSCIENTISTS & ENGINEERS

ORIGINAL ARTICLE

Performance of old and new mass-lumped triangular finite elements for wavefield modelling

W. A. Mulder[1,2]

[1]Shell Global Solutions International B.V., Den Haag, The Netherlands

[2]Department of Geoscience & Engineering, Faculty of Civil Engineering and Geosciences, Delft University of Technology, Delft, The Netherlands

Correspondence
W. A. Mulder, Shell Global Solutions International B. V., Carel van Bylandtlaan 30, 2596 HR Den Haag, The Netherlands.
Email: Wim.Mulder@shell.com

Abstract

Finite elements with mass lumping allow for explicit time stepping when modelling wave propagation and can be more efficient than finite differences in complex geological settings. In two dimensions on quadrilaterals, spectral elements are the obvious choice. Triangles offer more flexibility for meshing, but the construction of polynomial elements is less straightforward. The elements have to be augmented with higher-degree polynomials in the interior to preserve accuracy after lumping of the mass matrix. With the classic accuracy criterion, triangular elements suitable for mass lumping up to a polynomial degree 9 were found. With a newer, less restrictive criterion, new elements were constructed of degree 5–7. Some of these are more efficient than the older ones. To assess which of all these elements performs best, the acoustic wave equation is solved for a homogeneous model on a square and on a domain with corners, as well as on a heterogeneous example with topography. The accuracy and runtimes are measured using either higher-order time stepping or second-order time stepping with dispersion correction. For elements of polynomial degree 2 and higher, the latter is more efficient. Among the various finite elements, the degree-4 element appears to be a good choice.

KEYWORDS

acoustics, computing aspects, modelling, numerical study, seismics, wave

INTRODUCTION

The finite-element method can be attractive for solving the wave equation because irregular topography and large contrasts in material parameters do not necessarily have to degrade the spatial accuracy, as is the case with higher-order finite differences. Mass lumping avoids the cost of a lower-upper decomposition of the large sparse mass matrix. However, when applied to the regular polynomial elements on triangles or tetrahedra, mass lumping can lead to non-positive weights, causing instability of the explicit time stepping scheme. In addition, the spatial accuracy may decrease. These two problems can be avoided by enriching the element with higher-degree polynomials in the interior. Unlike spectral elements on quadrilaterals based on Legendre–Gauss–Lobatto points (Komatitsch & Vilotte, 1998; Orszag, 1980), the construction of higher-order continuous mass-lumped finite elements is not straightforward. So far, elements up to degree 9 on triangles have been found by various authors (Chin-Joe-Kong et al., 1999; Cohen et al., 2001; Crouzeix & Raviart, 1973; Cui et al., 2017; Liu et al., 2017; Mulder, 1996; Mulder, 2013; Tordjman, 1995).

The classic accuracy criterion for lumping of the mass matrix (Ciarlet, 1978, for instance) requires that polynomials up to a certain degree should be integrated exactly by the quadrature weights. That degree depends on the polynomial

TABLE 1 Element polynomial degree p, interior polynomial degree p', number of nodes per element n_p and the estimated Courant–Friedrichs–Lewy (CFL) number for the old and new elements. The results for the old elements have an asterisk. The letter or number before the colon denotes a version label in case more than one element was found for the given degree.

p	p'	n_p	CFL
1	1	3	1.14*
2	3	7	0.367*
3	4	12	0.210*
4	5	18	0.128*
5	7	30	0.0512*
			A:0.0747, B:0.0660, C:0.0635, D:0.0503, E:0.0366, F:0.0779, G:0.0661
6	9	46	D:0.0387*
	8	39	A:0.0404, B:0.0215
7	10	57	1:0.0288*, 2:0.00614*
			A:0.0253, B:0.00954, C:0.0333
8	11	69	0.0180*

degree of the element on the edges, the higher polynomial degree in its interior and the order of the partial differential equation. The lumped mass matrix is proportional to the weights.

Geevers et al. (2018b) proposed a sharper and less restrictive accuracy criterion, enabling the construction of tetrahedral elements that are significantly more efficient than the ones obtained with the classic criterion (Chin-Joe-Kong et al., 1999; Mulder, 1996). When applied to triangular elements, the less restrictive criterion provides the same elements for degree 2–4 as with the classic criterion but leads to infinitely many new elements of degree 5 and 7, whereas two were found for degree 6 (Mulder, 2022b).

Here, their relative performance will be examined on a homogeneous acoustic problem with a point source and on an inhomogeneous one with topography, in terms of the error as a function of the solution unknowns or degrees of freedom and as a function of the measured computing time. The latter provides an indication of the element's efficiency. The comparison is made for a number of traces rather than for all the unknowns, in contrast to a preliminary version (Mulder, 2022a).

With the second-order formulation of the wave equation, the numerical dispersion of a second-order time-stepping scheme will dominate the error for all but the linear element. This can be avoided by higher-order time stepping (von Kowalevsky, 1875; Lax & Wendroff, 1960; Dablain, 1986; Shubin & Bell, 1987) or Stork's dispersion correction (Anderson et al., 2015; Dai et al., 2014; Koene et al., 2018; Li et al., 2016; Mittet, 2017; Qin et al., 2017; Stork, 2013; Wang & Xu, 2015; Xu et al., 2017). Both approaches will be considered.

The next section briefly reviews the mass-lumped finite elements and the time-stepping scheme. Implementation details can be found in earlier publications (Mulder, 1996, 2001) and in textbooks on the finite element method (Cohen, 2002, for instance). Then, the numerical results are discussed in terms of the error as a function of the number of degrees of freedom and as a function of computing time. The required time to reach a certain accuracy serves as performance measure. The last section summarizes the main results.

REVIEW OF THE METHOD

Finite elements

The examples in this paper solve the acoustic wave equation in the second-order form:

$$\frac{1}{\rho c^2}\frac{\partial^2 u}{\partial t^2} - \nabla\cdot\left(\frac{1}{\rho}\nabla u\right) = f(t,\mathbf{x}) = w(t)\delta(\mathbf{x}-\mathbf{x}_s). \qquad (1)$$

Here the pressure $u(t,\mathbf{x})$ depends on the space coordinates $\mathbf{x}$ and time t, the material parameters are density $\rho(\mathbf{x})$ and sound speed $c(\mathbf{x})$ and the source $f(t,\mathbf{x})$ is a delta functions at $\mathbf{x}_s$ with wavelet $w(t)$. Initial values are $u(0,\mathbf{x}) = 0$ and $\partial_t u(0,\mathbf{x}) = 0$. In the accuracy tests, the influence of less than perfect absorbing boundary conditions is avoided by using either zero Dirichlet boundary conditions, where the pressure is zero on all boundaries, or zero Neumann boundary conditions, which are the natural boundary conditions with zero normal derivatives. The method can equally well be applied to the elastic wave equation (Geevers et al., 2018b; Geevers et al., 2019; Mulder & Shamasundar, 2016).

Finite-difference methods sample the solution on a regular grid. The spatial derivatives are approximated by fitting a polynomial through neighbouring solution values and evaluating its derivative at the desired point. Usually, polynomials of higher degrees are chosen to reduce the discretization error. Across discontinuities in the material parameters, the pressure

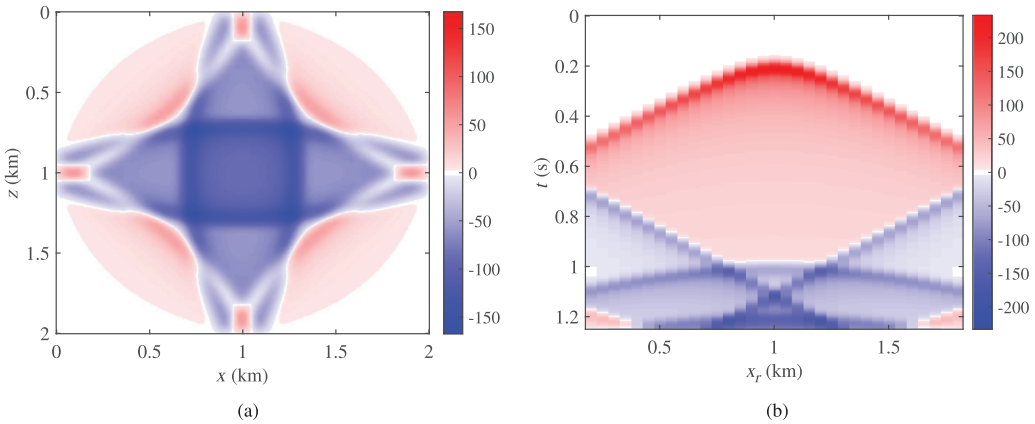

FIGURE 1 (a) Exact solution for a point source at the centre and reflecting boundaries. (b) Seismogram for a horizontal receiver line 200 m below the source.

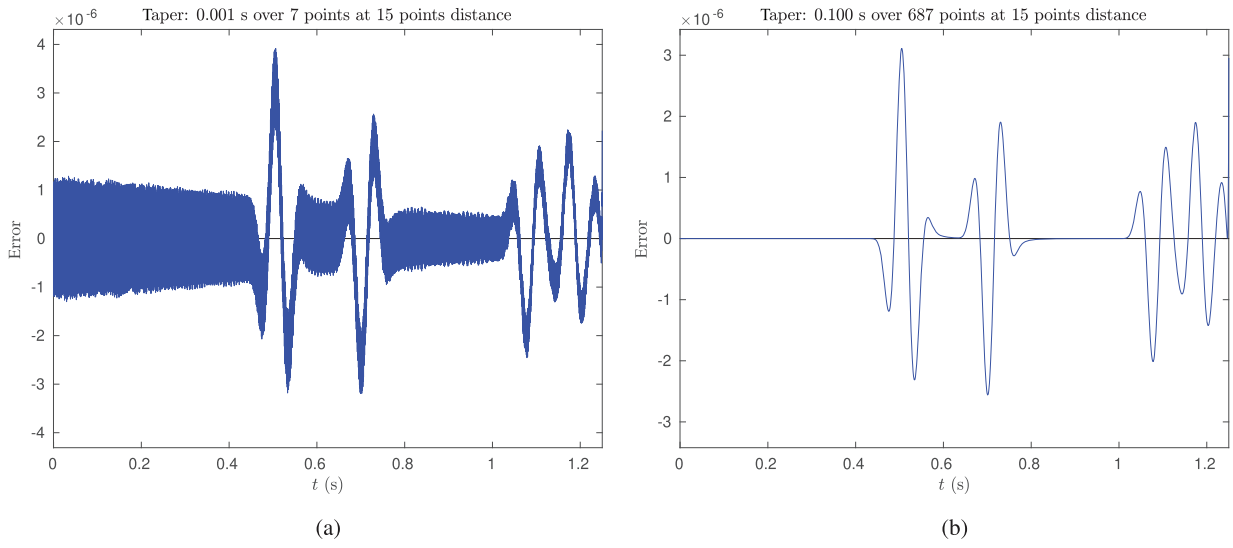

FIGURE 2 Effect of the taper width on the error. Noise appears for small width and decreases at larger width. The trace was extended by 0.001 s in panel (a) and 0.1 s in (b), but only the part of trace between 0 and 1.25 s is shown. There were 15 samples between 1.25 s and the onset of the taper.

is continuous but has a discontinuous derivative and causes a deterioration of the accuracy to second order in the grid spacing. On top of that, if the material parameters are just sampled on the grid, the unspecified position of an interface between the discontinuous materials will cause a first-order error.

Finite elements follow a different route towards discretization. The computational domain is divided up into small subsets $\mathcal{T}_j$ $(j = 1, \ldots, N_\mathcal{T})$ of, for instance, triangular or quadrilateral shape. A set of polynomials inside each of these is chosen to represent the solution. If polynomials of degree $p \geq 1$ are chosen on triangles, there are $\frac{1}{2}(p+1)(p+2)$ coefficients or degrees of freedom per element. After choosing a set of nodes $\mathbf{x}_\ell$ inside the triangle, the solution inside $\mathcal{T}_j$ can be expressed as $u_j(\mathbf{x}) = \sum_{k=1}^{p(p+1)/2} u_{j,k}\phi_{j,k}(\mathbf{x})$, where the Lagrange interpolating polynomials $\phi_{j,k}(\mathbf{x})$ are elements of the set $\boldsymbol{P}_p$ containing polynomials up to degree p and have the property $\phi_{j,k}(\mathbf{x}_\ell) = \delta_{k,\ell}$. Continuity across elements implies that the degree of freedom $u_{j,k}$ are shared between neighbouring elements if the nodes lay on the element edges or on the vertices. To have a unique one-dimensional polynomial representation on an edge, including the vertices at the endpoints, $p+1$ nodes are required, leaving $\frac{1}{2}p(p+1) - 3p = \frac{1}{2}(p-1)(p-2)$ for the interior.

With this representation, the spatial discretization follows from the substitution of $u(t, \mathbf{x}) = \sum_j u_j(t, \mathbf{x})$ into Equation (1) and integration against $\phi_{j',k'}(\mathbf{x})$. The result is

$$\mathbf{M}\partial_{tt}\mathbf{u} + \mathbf{K}\mathbf{u} = \mathbf{f}, \tag{2}$$

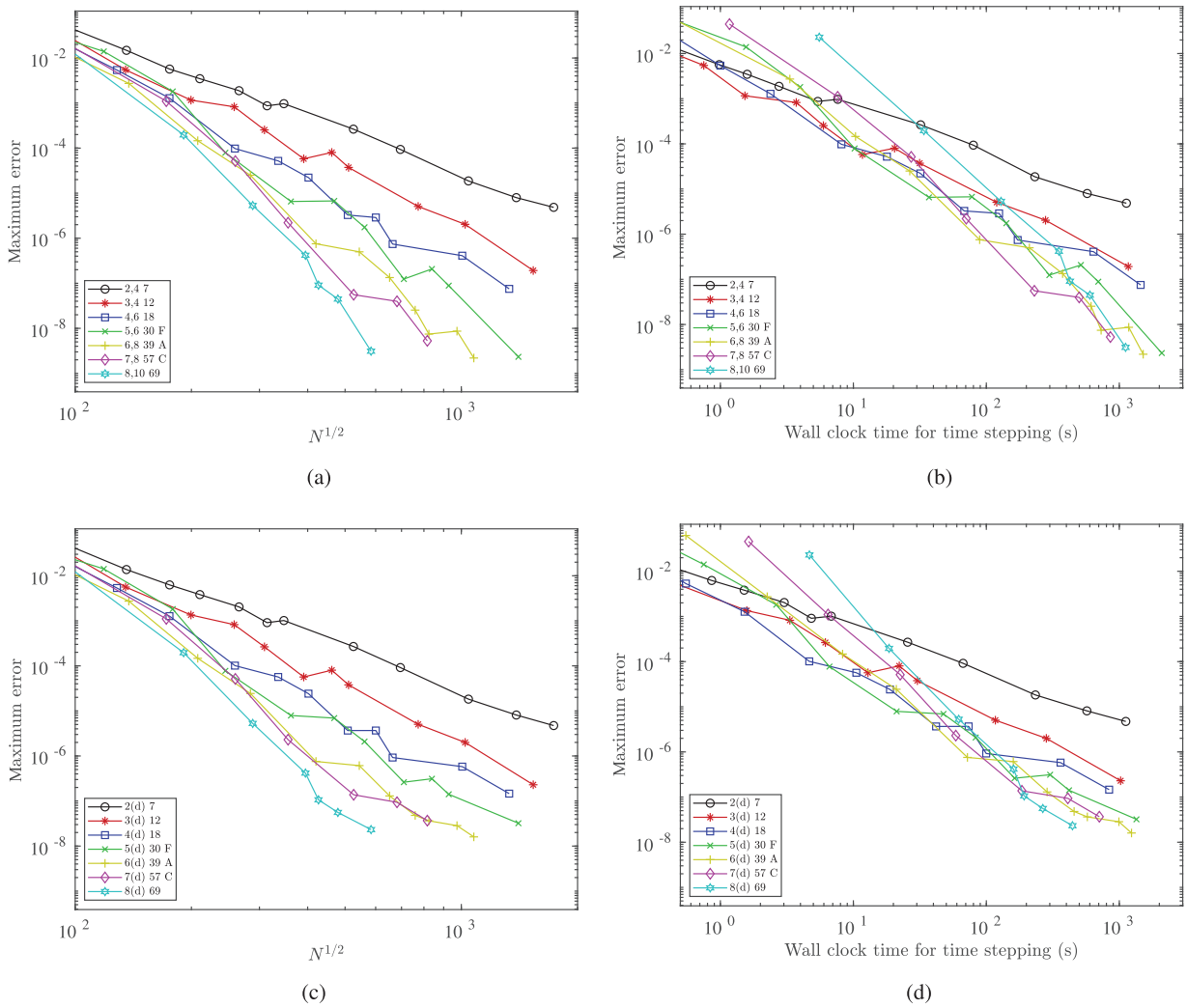

FIGURE 3 Convergence under mesh refinement for degree for degrees 2–8 with higher-order time stepping. The maximum error in the seismogram, scaled by the maximum value of the data, is plotted as a function of $N^{1/2}$, with N the total number of degrees of freedom (a,c). The panels on the right (b,d) depict errors as a function of the elapsed time for time stepping. The legend contains the degree and either the order for higher-degree time stepping (a,c) or dispersion correction (b,d) denoted by '(d)', followed by the number of nodes and the version name, if necessary.

with mass matrix $\mathbf{M}$, stiffness matrix $\mathbf{K}$, source vector $\mathbf{f}$ and solution $\mathbf{u}$, a vector that contains all N unknowns or degrees of freedom. The contribution to the mass matrix of a single element $\mathcal{T}_j$ is

$$\mathbf{M}_{\ell(j,k_1),\ell(j,k_2)} = \int_{\mathcal{T}_j} \mathrm{d}\mathbf{x}\, \frac{1}{\rho_j c_j^2} \phi_{j,k_1} \phi_{j,k_2}, \tag{3}$$

where $\ell(j,k)$ is the local-to-global map from indices k in element $\mathcal{T}_j$ to a global index $\ell(j,k)$ that takes care of the shared degrees of freedom at the element boundaries. The contribution to the stiffness matrix is

$$\mathbf{K}^{[m,n]}_{\ell(j,k_1),\ell(j,k_2)} = \int_{\mathcal{T}_j} \mathrm{d}\mathbf{x}\, \frac{1}{\rho_j} \frac{\partial \phi_{j,k_1}}{\partial x_m} \frac{\partial \phi_{j,k_2}}{\partial x_n} \quad (m,n = 1,2). \tag{4}$$

These contributions can then be combined into a global mass matrix and three stiffness matrices, but this is not done here. Instead, the mass matrix will be lumped and assembly of the stiffness matrices is carried out on the fly, as in Mulder (1996), Mulder and Shamasundar (2016) and others. In the current paper, ρ and c are assumed to be constant per element $\mathcal{T}_j$ for simplicity, but they may be discontinuous from one element to the other.

Mass lumping

The time discretization can be obtained with finite differencing in time, approximating $\partial_{tt}\mathbf{u}$ at time $t = n\Delta t$ by $(\mathbf{u}^{n+1} - 2\mathbf{u}^n + \mathbf{u}^{n+1})/\Delta t^2$ where $\mathbf{u}^n = \mathbf{u}(t^n, \mathbf{x})$. To avoid inversion of the global mass matrix at each time step, it may be lumped by replacing it by a diagonal matrix with its row sums, which is trivial to invert. The problem with that is a loss of spatial accuracy for triangular elements with polynomial degree $p > 1$. This can be repaired by augmenting the interior of the

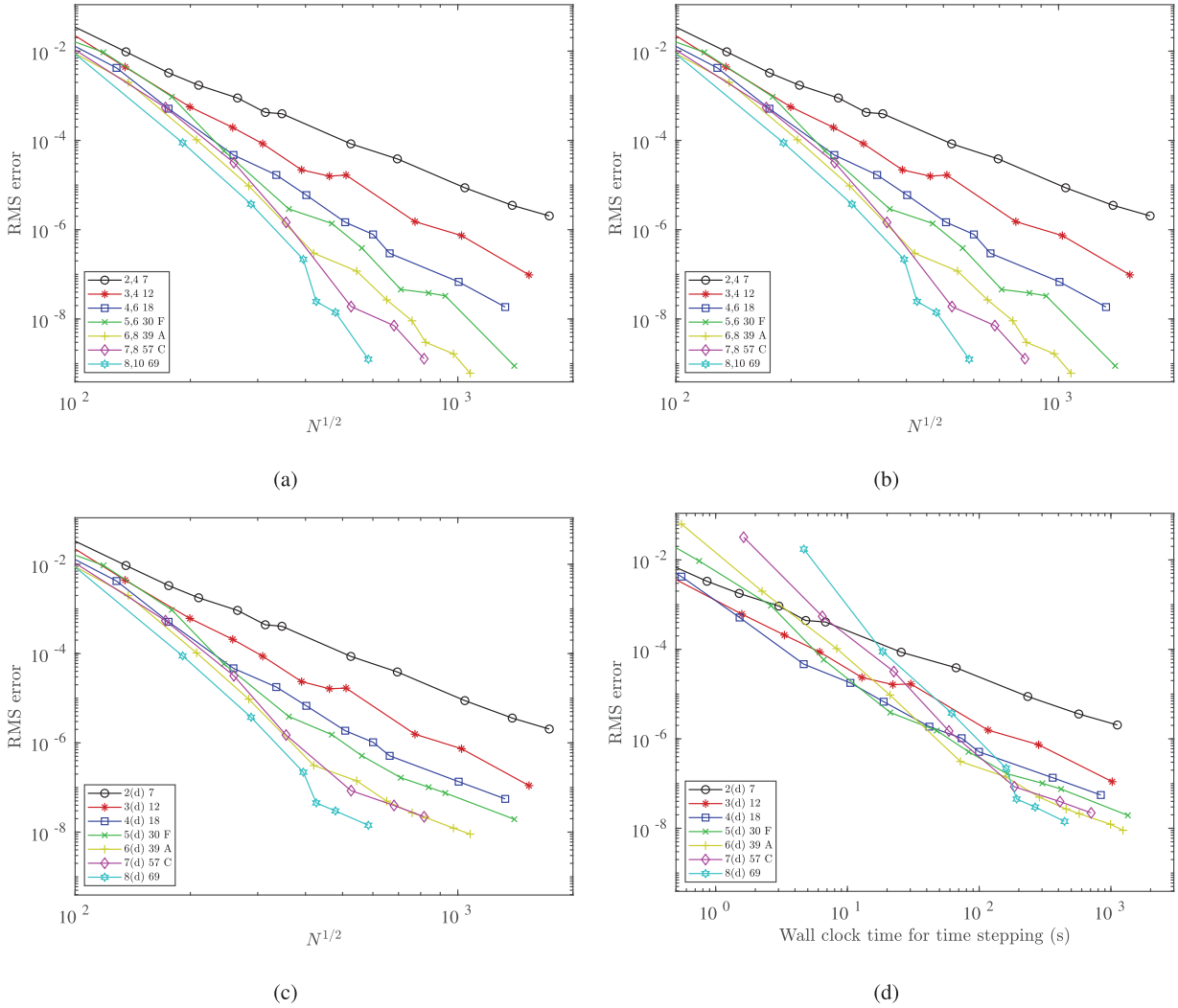

FIGURE 4 As Figure 3, but for the relative RMS error.

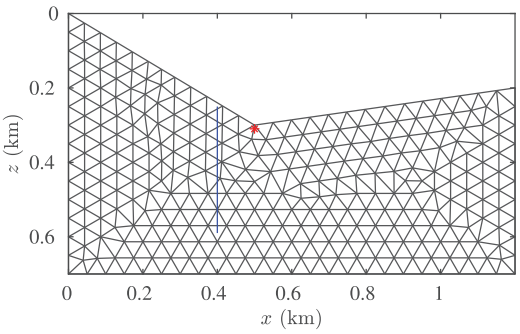

FIGURE 5 One of the meshes for the corner problem with the source position in red and receivers on the blue line.

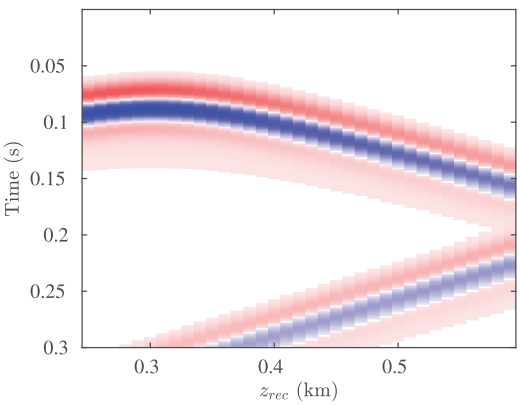

FIGURE 6 Seismogram as a function of time and receiver depth for the corner problem.

element with polynomials of a higher degree p'. In the case of the reference element with coordinates $\xi_{1,2} \in [0, 1]$, vertices (0,0), (0,1) and (1,0) and $\xi_0 = 1 - \xi_1 - \xi_2 \in [0, 1]$, the polynomials are of the form $b\phi(\xi_1, \xi_2)$ with bubble function $b = \xi_0\xi_1\xi_2$, a cubic polynomial that vanishes on the edges, and a polynomial $\phi(\xi_1, \xi_2) \in P_{p'-3}$. Note that with quadrilaterals, the Gauss–Lobatto nodes and Legendre polynomials can be chosen in each coordinate direction on the reference element,

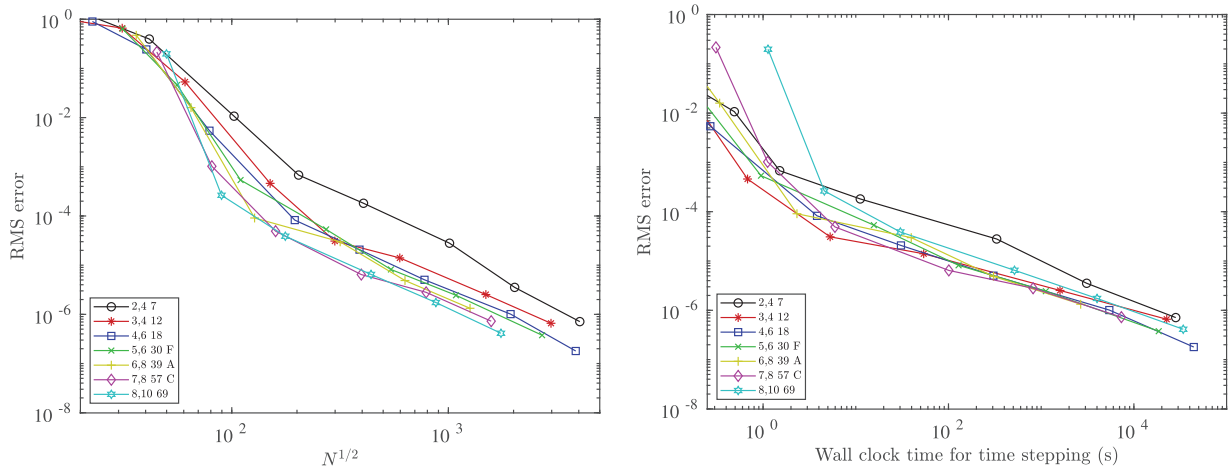

FIGURE 7 Relative RMS errors for degrees 2–8 with higher-order time stepping for the corner problem as a function of the square root of the number of degrees of freedom N (a) or computing time (b). The convergence deteriorates at smaller error values.

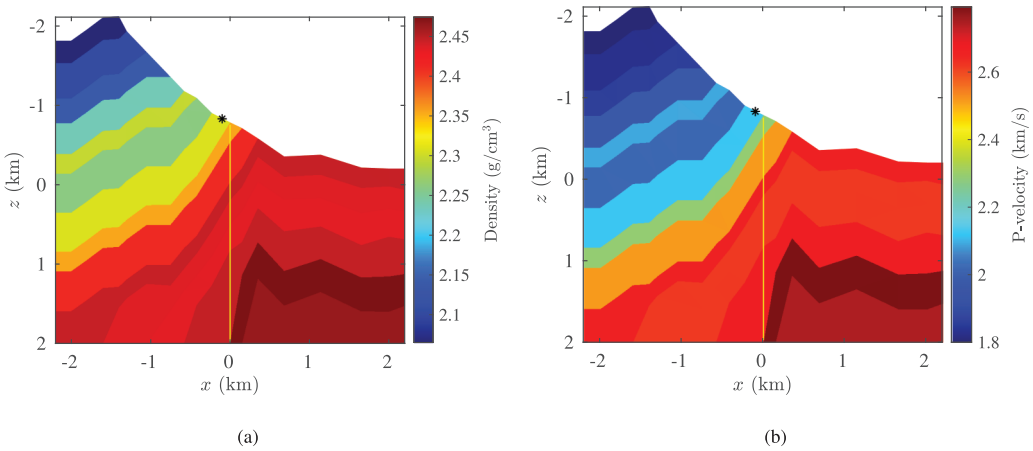

FIGURE 8 Model with density (a) and P-wave velocity (b) for the inhomogeneous problem.

a square, and do not suffer from loss of accuracy after mass lumping (Komatitsch & Vilotte, 1998; Mulder, 1999; Orszag, 1980).

A triangular element is characterized by its degree p on the edges and $p' \geq p$ in the interior, as well as the positions of the nodes that support the degrees of freedom. This leaves the problem of how to choose the nodes and degrees, subject to the following requirements. Continuity between elements is obtained for $p+1$ distinct points on each edge, two of which are the vertices. The nodes on each element are symmetrically arranged. Accuracy should be preserved after lumping. The lumped mass matrix consists of numerical quadrature weights, apart from a scaling factor, and these should be strictly positive to avoid time-stepping instabilities. The set of polynomials $U = \{b\} \otimes P_{p'-3}$, with degree p on the edges and p' in the interior of an element, should be unisolvent, that

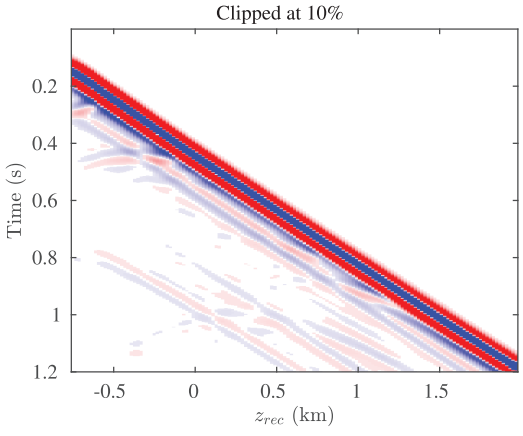

FIGURE 9 Seismogram as a function of time and receiver depth for the inhomogeneous problem.

is, the values on the nodes should define a unique Lagrange interpolating polynomial on each element (Cui et al., 2017; Marchildon & Zingg, 2022; Mulder, 2022b, 2023b).

The classic accuracy criterion requires numerical quadrature to be exact for polynomials of degree $p + p' - 2$. The less restrictive one (Geevers et al., 2018b; Mulder, 2022b) requires exact quadrature for polynomials in the set $P_{p-2} \otimes U$. In either case, the requirement that numerical quadrature is exact for the polynomials in the set leads to a nonlinear system of equations, which is linear in the quadrature weights but has coefficients that are polynomials in the parameters describing the node positions on the reference element.

This nonlinear system may have no solution or a finite or an infinite number of solutions, which are complex-valued in general. If the number of equations equals the number of unknowns, comprising the weights and node parameters, one may expect to have a finite number of solutions, although this is not always the case. If the number of complex-valued solutions is finite, it grows very rapidly with the degree and problem size and is bounded by the Bézout number (Li, 2003, for instance). If there are less equations than unknowns, an infinite number of solutions can be expected. An example with an infinite number of solutions is the degree-6 element obtained with the classic criterion (Mulder, 2013). Among the solutions, only the real-valued ones with strictly positive weights and node positions that do not lie outside the reference triangle are acceptable for mass lumping with the wave equation.

The less restrictive criterion was applied by Mulder (2022b) and led to the same elements as the classic one for degrees up to 4. For degrees 5 and 7, infinitely many elements were found. They have the same number of nodes as the old element. For degree 6, two new elements with less nodes were found. Table 1 summarizes results from Mulder (2013, 2022b) and Liu et al. (2017). These papers contain node positions and quadrature weights as well as pictures of the nodes for the reference elements.

In Mulder (2022b), the equations that prescribe exact quadrature for the degree-5 element comprise a set of 13 polynomial equations in 14 unknowns, seven for the quadrature weights and seven node parameters for the 30 nodes. The solution can be expressed as functions of one of the node parameters, which obeys a quartic equation. Two of its four roots provide useful solutions, each for a certain range of the parameter. To find a single solution, an additional constraint can be imposed, for instance, maximization of the Courant–Friedrichs–Lewy (CFL) number (Courant et al., 1928) that controls the maximum size of the time step. This led to an element labelled as version F for one of the roots of the quartic equation and version G for the other.

Likewise, there are 26 equations for 27 unknowns for degree 7 with an infinite number of solutions. The equations were solved with a Newton-type method starting with random initial solution values. Once a solution was found, the vector that characterizes the one-dimensional null space of the Jacobian of the polynomial system could be followed to find a larger CFL number. Version C was obtained in that way.

In the performance study, the degree-8 element of Cui et al. (2017) or Liu et al. (2017) is included. These elements are identical, which is not true for the degree-9 element. The one of Cui et al. (2017) actually has degree 10 instead of 9 on the edges. The element of Liu et al. (2017) has less nodes and the proper degree 9 on the edges. However, when trying to reproduce this element in Mathematica (Wolfram Research, Inc., 2016) with substantially extended precision, a modified Newton method starting from the values provided in the paper did not converge any further. Therefore, the element is not considered here.

Time stepping

The maximum allowable time step is controlled by the CFL number. For the finite elements, it can be estimated easily by considering a single element in natural coordinates (Mulder, 2013). This enables the initial screening of elements if more than one exists for a given degree and the number of nodes. In the actual simulations later on, the power method (von Mises & Pollaczek-Geiringer, 1929) is used instead because it provides a slightly sharper estimate.

Higher-order time stepping is obtained by removing error terms containing higher-order temporal derivatives that can be replaced by repeated application of the spatial operator. The approach goes by several names, such as the Cauchy–Kovalewski (von Kowalevsky, 1875) or Lax–Wendroff procedure (Lax & Wendroff, 1960), Dablain's scheme (Dablain, 1986) or the modified equation approach (Shubin & Bell, 1987). Although the CFL number increases for higher orders (Mulder, 2013, for instance), the larger time step does not compensate for the increased cost of repeatedly applying the spatial operator. Here, the time-stepping order M_t is chosen as the smallest even number $M_t \geq p + 1$: $M_t = 2\,\mathrm{floor}(p/2 + 1)$.

An alternative is Stork's dispersion correction (Stork, 2013), which is based on the observation that second-order time stepping is exact but at the wrong frequency. The time-stepping error can be removed by mapping an observed time series at the receiver to the correct frequency. Among several implementations, the one suggested by Koene et al. (2018) is chosen, employing Fourier interpolation on the time series.

PERFORMANCE

A measure for an element's performance is the computing time required to reach a given accuracy of the solution. The

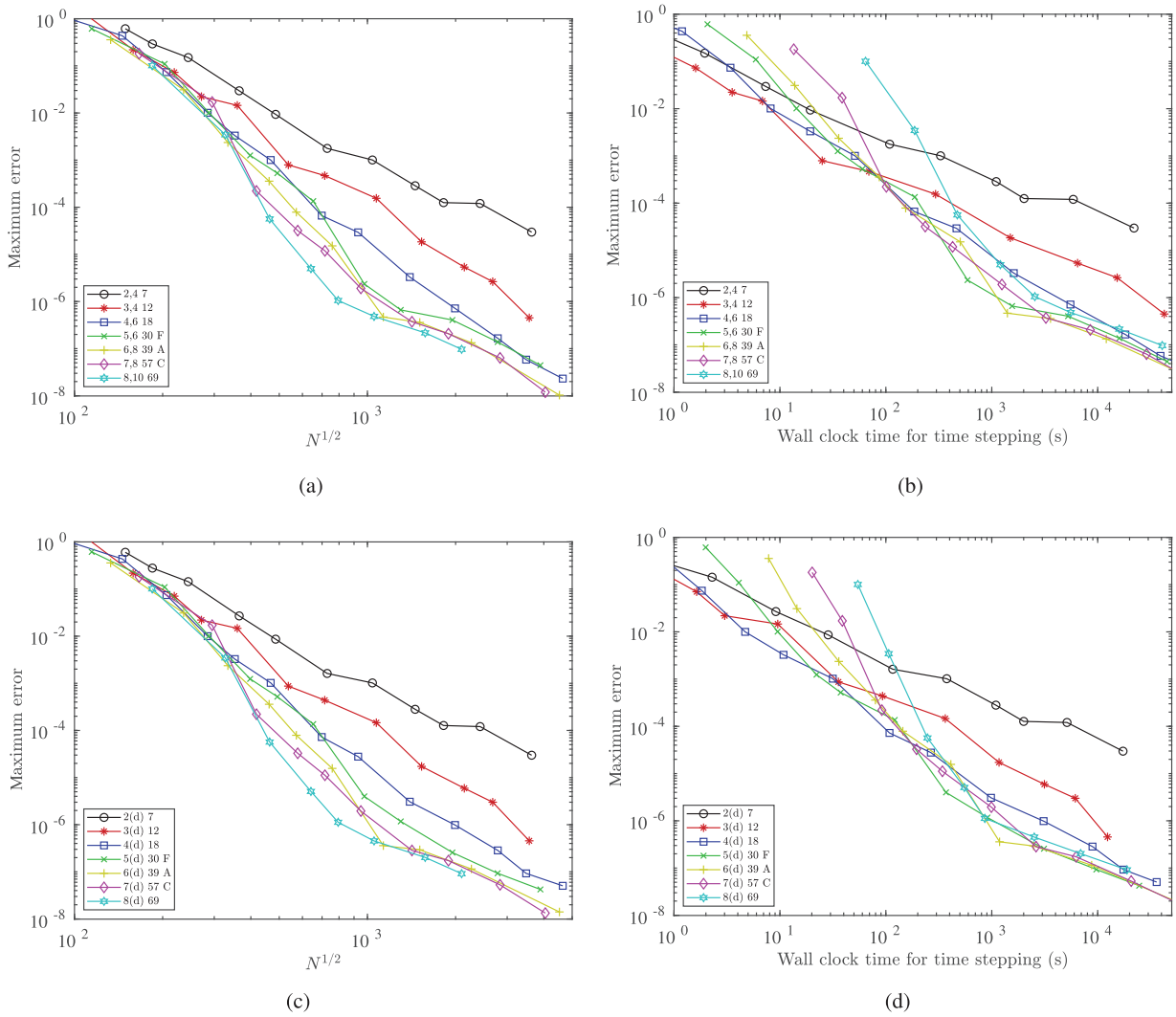

FIGURE 10 Relative maximum errors for the inhomogeneous problem for degrees 2–8 with higher-order time stepping (a,b) or dispersion correction (c,d) for the inhomogeneous problem as a function of the square root of the number of degrees of freedom N (a,c) or computing time (b,d). The convergence deteriorates when the error drops below about 10^{-6}.

efficiency is determined by several factors. A larger Courant–Friedrichs–Lew (CFL) number will decrease the number of required time steps. Table 1 lists estimates taken from earlier papers (Mulder, 2013, 2022b). The values of the CFL number are based on a single element with natural boundary conditions for degrees 1–8. The asterisk marks values for elements obtained with the old accuracy criterion. If multiple elements were found, a version label is included as a single letter or number, followed by a colon and the CFL number estimate. Table 1 shows that the CFL number and its corresponding maximum time step decrease for elements of higher degree. This will lower their efficiency. The increased number of nodes per element and the decreasing CFL number have to be compensated by using elements of larger size, and it is expected that there is an optimum for some intermediate degree. In addition, simple models may allow for large elements, but complex models with fine details may require small elements for a proper representation, which naturally would favour elements of a lower degree. The goal of the current paper is to gain a rough idea of which element and degree provides the best overall accuracy for a given amount of computing time.

The spatial discretization error is expected to behave as Ch^{p+1} with element size h and error constant C. Among elements of the same degree, the constant C may be quite different for each version and will depend on the problem. Because of that, a larger CFL number does not necessarily imply a better performance.

Given these considerations, it is not straightforward to predict the actual performance. Therefore, numerical tests were performed on a homogeneous test problem with an exact solution to obtain some insight into the relative efficiency of the various elements. If there are multiple versions of an element, only those for the most efficient one will be shown,

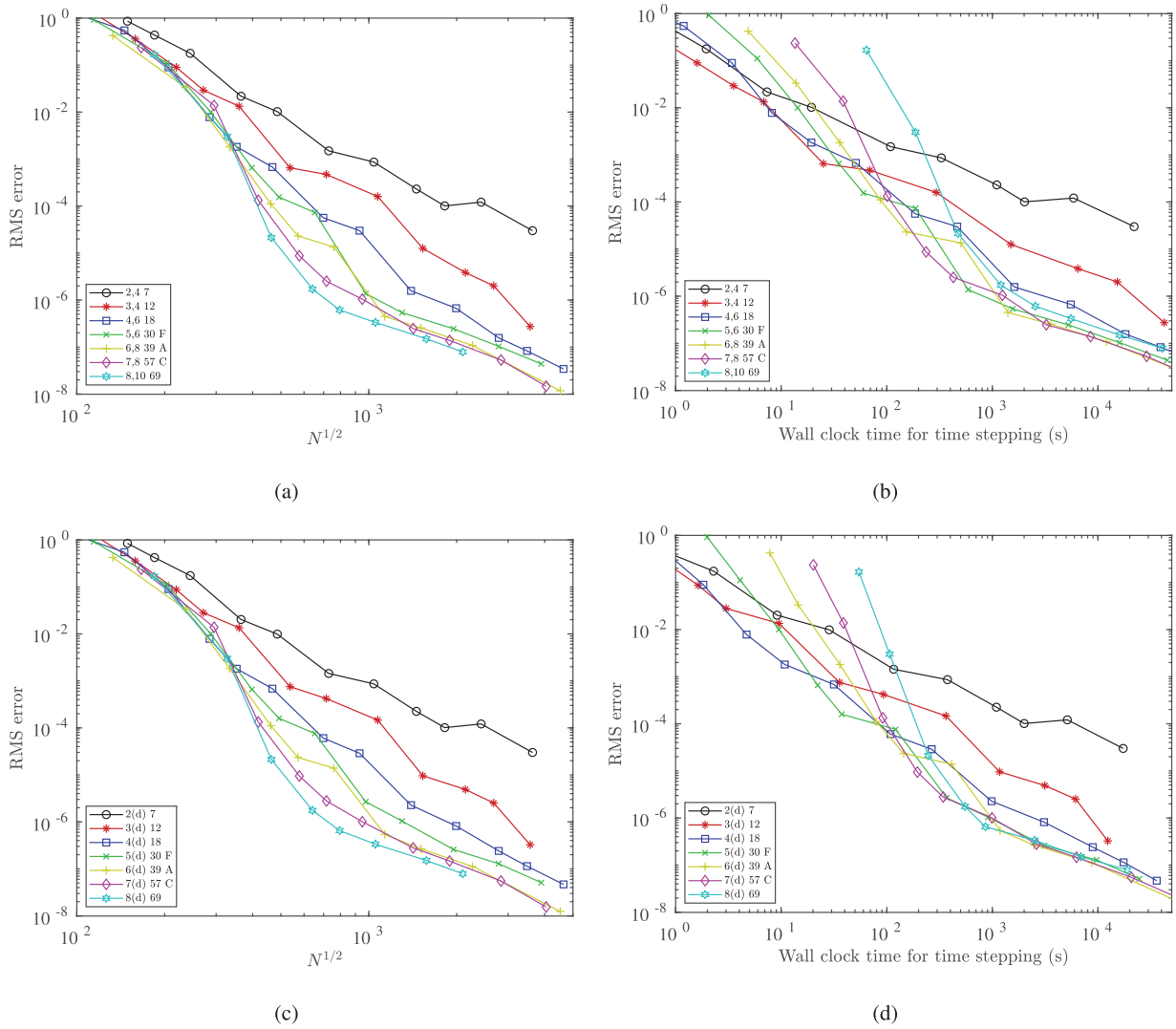

FIGURE 11 As Figure 10 but for the RMS errors, showing a similar deterioration of the convergence below about 10^{-6}.

namely version F for the 30-node degree 5, version A for the 39-node degree-6 element, and version C for the 57-node degree-7 element.

Homogeneous problem

The test problem consists in solving the acoustic wave equation (1) for a homogeneous problem with a delta-function source at $\mathbf{x}_s$ (c.f. Mulder, 2020). The domain is a square with sides of 2 km. Zero Dirichlet boundary conditions are imposed on all sides. The sound speed $c = 2$ km/s and the density $\rho = 2$ g/cm^3. The point source at the centre has a wavelet

$$w(t) = \begin{cases} \left[4(t/T_w)\{1-(t/T_w)\}\right]^q, & t \in (0, T_w), \\ 0, & t \notin (0, T_w), \end{cases} \tag{5}$$

and in this example, $T_w = 0.2$ s. The power $q = 16$ is chosen large enough to avoid a discontinuity in the higher derivatives at the start and end of the wavelet, which would otherwise reduce the accuracy. Note that a Ricker wavelet is infinitely many times differentiable and does not have this problem, but is not bounded in time, although in practice it is truncated to where the amplitudes drop below machine precision.

Figure 1a displays the solution at time $t_{\max} = 1.25$ s for a source at $x_s = z_s = 1$ km. Figure 1b shows the seismogram for receivers between $x_r = 200$ and 1800 m at a 50-m interval and a depth $z_r = 1200$ m.

The error in the numerical solution is measured by the relative maximum error, defined as the maximum absolute value of the error over all traces divided by the maximum value of the recorded values. The computations were carried out in double precision (16 digits).

The maximum time step for second-order time stepping is taken as $\Delta t_{\max} = \sqrt{2/\sigma_{\max}}$, where $\sigma_{\max}$ is the maximum eigenvalue of the spatial operator, the product of the inverse diagonal mass matrix and the stiffness matrix. The power

method (von Mises & Pollaczek-Geiringer, 1929) provided an estimate of $\sigma_{\max}$ for each run. The results turned out to be only slightly larger, by a few percen than the crude estimates in Table 1, obtained on a single reference element with natural boundary conditions. As mentioned before, $\Delta t_{\max}$ should be increased by a given factor for higher-order time stepping.

Note that the sampling criterion for dispersion correction for a maximum frequency $f_{\max}$ is $\Delta t \leq 1/(\pi f_{\max})$, smaller than the usual Nyquist bound $\Delta t \leq 1/(2 f_{\max})$ (Koene et al., 2018). Here, the maximum time step in the simulations was limited to $\Delta t \leq 4$ ms, corresponding to about 80 Hz with the first sampling criterion. At this frequency, the amplitude of the wavelet has decreased well below 10^{-10}, relative to its maximum at zero frequency.

The zero frequency in the wavelet causes problems with the implementation of dispersion correction by Koene et al. (2018). At the maximum recording time, the recorded signal is cut off abruptly and this leads to large errors towards the end of the trace. To avoid this problem, the recording time was extended beyond $t_{\max}$ and the tail of the recorded data was tapered to zero, with a smooth taper of the form $\xi^2(3-2\xi)$, $0 < \xi < 1$, where ξ decreases linearly from 1 at a number of samples beyond $t_{\max}$ down to zero at the end of the trace. Then, the dispersion correction was applied and the result truncated to $t_{\max} = 1.25$ s. To avoid large errors around that time, the taper should start at a larger time value, at some distance beyond $t_{\max}$. Figure 2 illustrates how the taper length affects the error. In Figure 2a, the taper is a width of about 1 ms or seven sample points and starts at 15 samples beyond $t_{\max}$. The noise and signal are similar in size. With a taper width of 10 ms, involving 687 samples and starting at 15 samples beyond $t_{\max}$, the noise is no longer visible in Figure 2b. The following results are based on a rather large taper length of 0.19 s, starting at $t_{\max} + 0.01$ s. A similar extension is applied at the start of the wavelet, adversely affecting the efficiency of the dispersion correction. The advantage of this generous choice is that the same tapering parameters can be used in all simulations, but the disadvantage is that the computing times are larger than strictly necessary. This should be kept in mind when judging the convergence results.

Figure 3a displays convergence results for the degree-2 to degree-8 elements. The total number of degrees of freedom, including the zero boundary values, is denoted by N. In two dimensions, the average element size $h \propto N^{-1/2}$. The relative maximum error is plotted as a function of $N^{1/2}$. The slope of the curves on average follows the expected convergence rate of $N^{-1/2(p+1)}$. To translate this result into the finite-element equivalent of points per wavelength, a frequency of 20 Hz is taken, where the spectrum of the wavelet has dropped to 10% of its maximum value. With a sound speed of 2 km/s and sides of 2 km, the domain contains 20 wavelengths in the horizontal or vertical direction and about $N^{1/2}/20$ nodes per wavelength.

Figure 3b shows the relative maximum error as a function of the observed wall clock time for the higher-order time stepping, measured only for the time-stepping part of the run and averaged over five runs. The C code dates back to 1995 and was at the time used to prepare the material for Mulder (1996). The observed times are not at all representative of what can be obtained on modern hardware but are still useful for a relative comparison. Figures 3c and 3d display similar results for second-order time stepping and dispersion correction. When the errors become very small, around 10^{-7} to 10^{-8}, the results are not as accurate as with the more robust higher-order time stepping, but the computing cost is significantly smaller. Figure 4 shows similar results for the relative root-mean-square (RMS) error. The results suggest that the degree-4 element is a good choice for an accuracy down to 10^{-4} to 10^{-5} in this simple example.

Corners

The homogeneous problem on the square confirms the expected convergence behaviour with errors of the form Ch^{p+1}, where the mesh size h is proportional to $N^{-1/2}$ for a number of degrees of freedom N. In general, however, this convergence is not obtained, for various reasons. One is the lack of regularity of the wavelet, but that is avoided here by choosing a wavelet that is sufficiently many times differentiable in time. If the finite-element mesh does not follow the interfaces between different materials, where the model parameters are discontinuous, the convergence degrades. The same may happen with large variations of the material parameters inside an element. Distorted meshes (Geevers et al., 2018a), sharp pinch-outs, thin layers, curved interfaces and very rough surfaces can cause problems and may require some form of homogenization to avoid elements much smaller than the modelled wavelengths.

Corner singularities (Tschöke & Gravenkamp, 2018, for instance) in the topography or at material interfaces can also adversely affect convergence. As an illustration of the latter, Figure 5 shows a coarser mesh for a homogeneous test problem with zero Neumann or natural boundary conditions all around. The sound speed is 3 km/s, and the density is 2 g/cm^3. The wavelet is taken as the second time derivative $w''(t)$ of Equation (5) with a power $q = 16$ and length $T_w = 0.1$ s. The source is located at $x_s = 500$ m and $z_s = 310$ m. The vertical receiver line at $x_r = 400$ m starts at $z_r = 250$ m and ends at $z_r = 590$ m with a 10-m spacing. Figure 6 displays the seismogram. The convergence under mesh refinement in Figure 7 with higher-order time stepping for elements for degree 2–8 initially shows the expected behaviour, but the convergence of the relative RMS error breaks down around about 10^{-4} to hardly better than second order.

The wavelet has a peak frequency of 26 Hz, and its amplitude has dropped by 10% at 54 Hz. The corresponding wavelengths are 56 and 115 m. With an area of 0.59 km^2, this amounts to $N^{1/2}/14$ or $N^{1/2}/6.7$ nodes per wavelength.

Inhomogeneous example

Figure 8 displays a model for an acoustic test problem, the same as in Mulder (2023a). The shot at $x_s = 100$ m and 6-m depth is indicated by a black star and the receiver positions by the yellow line with $x_r = 0$ m and z_r from −750 to 1970 m with a 20-m spacing. The wavelet is the second time derivative $w''(t)$ of Equation (5) with a power $q = 16$ and length $T_w = 0.2$ s, different from the one in Mulder (2023a). Traces are recorded up to 1.2 s. Figure 9 shows the seismogram, clipped at 10% of its peak amplitude.

The errors were estimated by comparing it to a solution on a very fine mesh. Figures 10 and 11 display the relative maximum and RMS errors. Convergence is reasonable down to around 10^{-6} and then slows down. Again, the degree-4 element performs quite well. Only for errors below 10^{-4}, the higher-degree elements become more efficient in this example.

CONCLUSIONS

The efficiency of two-dimensional continuous mass-lumped finite elements on triangles was studied for elements of degrees 2–8, including newer elements of degree 5–7 obtained with a sharper and less restrictive accuracy criterion for mass lumping than the classic one. There may, however, exist more efficient elements of higher degree.

Three acoustic test problems were considered. The first is a homogeneous example on a square domain and exhibits the expected convergence behaviour in terms of element size. The higher-degree elements are more accurate than those of lower degrees but are most costly because they have a larger number of nodes and impose smaller time steps. For a relative accuracy of around 0.01% or larger, the degree-4 element appears to be a good choice. The second test problem is also homogeneous but has simple topography and as such will be impacted by the notorious corner singularities. The convergence tests on a sequence of successively finer meshes initially show the same convergence as would be obtained on a rectangular domain but deteriorates at smaller relative root-mean-square errors, below 0.01%. In this case, the degree-4 element again performs well. The third example is a check-shot problem with a more complex topography and layers with different properties, although still piecewise constant per layer. Again, the degree-4 element appears to be the most attractive for an accuracy of 0.01% or larger.

DATA AVAILABILITY STATEMENT

Data sharing is not applicable to this article as no new data were created or analysed in this study. However, if the computational results shown in the figures are considered as new data, then the author elects not to share those.

ORCID

W. A. Mulder https://orcid.org/0000-0001-7020-9297

REFERENCES

Anderson, J.E., Brytik, V. & Ayeni, G. (2015) Numerical temporal dispersion corrections for broadband temporal simulation, RTM and FWI. In *SEG Technical Program Expanded Abstracts*. Houston, TX: Society of Exploration Geophysicists, pp. 1096–1100.

Chin-Joe-Kong, M.J.S., Mulder, W.A. & van Veldhuizen, M. (1999) Higher-order triangular and tetrahedral finite elements with mass lumping for solving the wave equation. *Journal of Engineering Mathematics*, 35, 405–426.

Ciarlet, P.G. (1978) *The finite element method for elliptic problems*, Studies in Mathematics and Its Applications, volume 4. Amsterdam, The Netherlands: North-Holland.

Cohen, G., Joly, P., Roberts, J.E. & Tordjman, N. (2001) Higher order triangular finite elements with mass lumping for the wave equation. *SIAM Journal on Numerical Analysis*, 38(6), 2047–2078.

Cohen, G.C. (2002) *Higher-order numerical methods for transient wave equations*. Berlin, Germany: Springer.

Courant, R., Friedrichs, K. & Lewy, H. (1928) Über die partiellen Differenzengleichungen der mathematischen Physik. *Mathematische Annalen*, 100(1), 32–74.

Crouzeix, M. & Raviart, P.-A. (1973) Conforming and non conforming finite element methods for solving the stationary Stokes equations. *Revue française d'automatique informatique recherche opérationnelle. Analyse numérique*, 7(R3), 33–75.

Cui, T., Leng, W., Lin, D., Ma, S. & Zhang, L. (2017) High order mass-lumping finite elements on simplexes. *Numerical Mathematics: Theory, Methods and Applications*, 10(2), 331–350.

Dablain, M.A. (1986) The application of high-order differencing to the scalar wave equation. *Geophysics*, 51(1), 54–66.

Dai, N., Wu, W. & Liu, H. (2014) Solutions to numerical dispersion error of time FD in RTM. In *SEG Technical Program Expanded Abstracts 2014*. Houston, TX: Society of Exploration Geophysicists, pp. 4027–4031.

Geevers, S., Mulder, W.A. & van der Vegt, J.J.W. (2018a) Dispersion properties of explicit finite element methods for wave propagation modelling on tetrahedral meshes. *Journal of Scientific Computing*, 77(1), 372–396.

Geevers, S., Mulder, W.A. & van der Vegt, J.J.W. (2018b) New higher-order mass-lumped tetrahedral elements for wave propagation modelling. *SIAM Journal on Scientific Computing*, 40(5), A2830–A2857.

Geevers, S., Mulder, W.A. & van der Vegt, J.J.W. (2019) Efficient quadrature rules for computing the stiffness matrices of mass-lumped tetrahedral elements for linear wave problems. *SIAM Journal on Scientific Computing*, 41(2), A1041–A1065.

Koene, E.F.M., Robertsson, J.O.A., Broggini, F. & Andersson, F. (2018) Eliminating time dispersion from seismic wave modeling. *Geophysical Journal International*, 213(1), 169–180.

Komatitsch, D. & Vilotte, J.P. (1998) The spectral-element method: an efficient tool to simulate the seismic response of 2-D and 3-D geological structures. *Bulletin of the Seismological Society of America*, 88(2), 368–392.

Lax, P. & Wendroff, B. (1960) Systems of conservation laws. *Communications on Pure and Applied Mathematics*, 31(2), 217–237.

Li, T.Y. (2003) Numerical solution of polynomial systems by homotopy continuation methods. In *Handbook of Numerical Analysis*, volume 11. Amsterdam: Elsevier, pp. 209–304.

Li, Y.E., Wong, M. & Clapp, R. (2016) Equivalent accuracy at a fraction of the cost: overcoming temporal dispersion. *Geophysics*, 81(5), T189–T196.

Liu, Y., Teng, J., Xu, T. & Badal, J. (2017) Higher-order triangular spectral element method with optimized cubature points for seismic wavefield modeling. *Journal of Computational Physics*, 336, 458–480.

Marchildon, A.L. & Zingg, D.W. (2022) Unisolvency for polynomial interpolation in simplices with symmetrical nodal distributions. *Journal of Scientific Computing*, 92(2), 1–24.

Mittet, R. (2017) On the internal interfaces in finite-difference schemes. *Geophysics*, 82(4), T159–T182.

Mulder, W.A. (1996) A comparison between higher-order finite elements and finite differences for solving the wave equation. In Désidéri, J.-A., LeTallec, P., Oñate, E., Périaux, J. & Stein, E. (Eds.), *Proceedings of the Second ECCOMAS Conference on Numerical Methods in Engineering*, Chichester, U.K.: John Wiley & Sons, pp. 344–350.

Mulder, W.A. (1999) Spurious modes in finite-element discretisations of the wave equation may not be all that bad. *Applied Numerical Mathematics*, 30(4), 425–445.

Mulder, W.A. (2001) Higher-order mass-lumped finite elements for the wave equation. *Journal of Computational Acoustics*, 9(2), 671–680.

Mulder, W.A. (2013) New triangular mass-lumped finite elements of degree six for wave propagation. *Progress in Electromagnetics Research*, 141, 671–692.

Mulder, W.A. (2020) On the error behaviour of force and moment sources in simplicial spectral finite elements. *Geophysical Prospecting*, 68, 2598–2603.

Mulder, W.A. (2022a) Efficiency of old and new triangular finite elements for wavefield modelling in time. In *83rd EAGE Conference and Exhibition 2022, Extended Abstracts*. Houten, the Netherlands: European Association of Geoscientists & Engineers, Volume 2022, pp. 1–5.

Mulder, W.A. (2022b) More continuous mass-lumped triangular finite elements. *Journal of Scientific Computing*, 92(2), 38.

Mulder, W.A. (2023a) Temporal dispersion correction for wave-propagation modelling with a series approach. *Geophysical Prospecting*. Submitted.

Mulder, W.A. (2023b) Unisolvence of symmetric node patterns for polynomial spaces on the simplex. *Journal of Scientific Computing*, 95(2), 1–25. https://doi.org/10.1007/s10915-023-02161-1

Mulder, W.A. & Shamasundar, R. (2016) Performance of continuous mass-lumped tetrahedral elements for elastic wave propagation with and without global assembly. *Geophysical Journal International*, 207(1), 414–421.

Orszag, S.A. (1980) Spectral methods for problems in complex geometries. *Journal of Computational Physics*, 37(1), 70–92.

Qin, Y., Quiring, S. & Nauta, M. (2017) Temporal dispersion correction and prediction by using spectral mapping. In *79th EAGE Conference & Exhibition, Paris, France, Extended Abstracts, Th P1 10*. Houten, the Netherlands: European Association of Geoscientists & Engineers, Volume 2017, pp. 1–5.

Shubin, G.R. & Bell, J.B. (1987) A modified equation approach to constructing fourth order methods for acoustic wave propagation. *SIAM Journal on Scientific and Statistical Computing*, 8(2), 135–151.

Stork, C. (2013) Eliminating nearly all dispersion error from FD modeling and RTM with minimal cost increase. In *75th EAGE Conference & Exhibition incorporating SPE EUROPEC, Extended Abstract*. Houten, the Netherlands: European Association of Geoscientists & Engineers, cp-348-01021.

Tordjman, N. (1995) *Élements finis d'order élevé avec condensation de masse pour l'equation des ondes*. PhD thesis, L'Université Paris IX Dauphine.

Tschöke, K. & Gravenkamp, H. (2018) On the numerical convergence and performance of different spatial discretization techniques for transient elastodynamic wave propagation problems. *Wave Motion*, 82, 62–85.

von Kowalevsky, S. (1875) Zur Theorie der partiellen Differentialgleichung. *Journal für die reine und angewandte Mathematik*, 80, 1–32.

von Mises, R. & Pollaczek-Geiringer, H. (1929) Praktische Verfahren der Gleichungsauflösung. *Zeitschrift für Angewandte Mathematik und Mechanik*, 9(2), 152–164.

Wang, M. & Xu, S. (2015) Time dispersion transforms in finite difference of wave propagation. In *77th EAGE Conference & Exhibition, Extended Abstract*. Houten, the Netherlands: European Association of Geoscientists & Engineers, Volume 2015, pp. 1–5.

Wolfram Research, Inc. (2016) *Mathematica*, Version 10.4. Champaign, IL.

Xu, Z., Jiao, K., Cheng, X., Sun, D., King, R., Nichols, D. & Vigh, D. (2017) *Time-dispersion filter for finite-difference modeling and reverse time migration*. In *SEG Technical Program Expanded Abstracts 2017*. Houston, TX: Society of Exploration Geophysicists, pp. 4448–4452.

How to cite this article: Mulder, W. A. (2024) Performance of old and new mass-lumped triangular finite elements for wavefield modelling. *Geophysical Prospecting*, 72, 885–896. https://doi.org/10.1111/1365-2478.13383